Journal of Materials Chemistry A

PAPER

Nanocapsules Containing Salt Hydrate Phase Change Materials for Thermal Energy Storage

Received 00th January 20xx,
Accepted 00th January 20xx

DOI: 10.1039/x0xx00000x

www.rsc.org/

Michael Graham*, Elena Shchukina, Paula Felix De Castro and Dmitry Shchukin

Abstract

Thermal energy storage has many important applications, and is most efficiently achieved by latent heat storage using phase change materials (PCMs). Salt hydrates have advantages such as high energy storage density, high latent heat and incombustability. However, they suffer from drawbacks such as incongruent melting and corrosion of metallic container materials. By encapsulating them in a polymer shell, problems can be eliminated. Here we demonstrate a simple method to nanoencapsulate magnesium nitrate hexhydrate, employing an *in situ* miniemulsion polymerisation with ethyl-2-cyanoacrylate as monomer. Using sonication to prepare miniemulsions improved the synthesis by reducing the amount of surfactant required as stabiliser. Thermal properties were analysed by differential scanning calorimetry (DSC) and thermogravimetric analysis (TGA). Fourier transform infrared spectroscopy (FTIR) was employed to prove the presence of salt hydrate within the nanocapsules. Results show the capsules are 100-200nm in size, have salt hydrate located in the core and are stable over at least 100 thermal cycles with only a 3% reduction in latent heat. Supercooling is also drastically reduced. To the best of our knowledge, this is the first time an encapsulated salt hydrate PCM has been proven to have a lifetime of 100+ heat uptake/release cycles.

Introduction

Storage of energy is essential due to increasing global energy demand. Phase change materials (PCMs) are efficient at storing large amounts of thermal energy quasi-isothermally during phase transition[1,2]. This process is known as latent heat storage, and gives storage density approximately 10 times higher than that of commonly used sensible heat storage materials such as rock or water[3,4]. Increased efficiency also means smaller storage units are required, reducing cost and spatial requirements. PCM applications include storage for concentrated solar power plants[5,6], passive air conditioning[7,8] and thermal management of devices such as photovoltaics[9,10] and electronics[7,11,12]. The most promising class of PCMs are inorganic salt hydrates. Major advantages are their extremely high energy storage density, wide range of melting temperatures and low cost[7,13–15]. They also avoid disadvantages of organic PCMs (paraffin waxes), which are flammable[16] and odourous[17,18]. However, salt hydrates are chemically unstable due to incongruent melting, have a tendency to supercool and are corrosive towards metals used for heat transfer[3,13,19].

To overcome these obstacles, it is necessary to isolate PCMs *i.e.* to encapsulate them. Encapsulation is a process of enclosing an active material within a shell. Polymers are widely used shell materials due to good strength and flexibility[20]. Encapsulation has been applied to many active ingredients, such as corrosion inhibitors[21,22], drugs[23–25] and DNA[26]. A general way to produce capsules is to create an emulsion with the active material in the dispersed phase. Polymerisation can then take place at the emulsion droplet interface. The term emulsion generally refers to a system of oil droplets dispersed in water. A system with water droplets dispersed in oil is known as an inverse emulsion. To obtain smaller droplet sizes, emulsions can be sheared to create a miniemulsion. Although there are many encapsulation methods[27–30], only miniemulsion polymerisation can provide capsules with a diameter less than 500nm on a large scale[31]. Encapsulating PCMs gives benefits such as larger heat transfer area and increased thermal cycling stability, which has been proven with research on organic PCMs[32–35].

Salt hydrates are difficult to encapsulate due to their hydrophilicity and tendency to alter their water content[36,37]. Despite this, several examples of their encapsulation have been reported in literature. Platte *et al*[37] encapsulated several salt hydrate mixtures. The capsules of approximately 45µm diameter were made using ORMOCER polymers, which have inorganic and organic moieties covalently bonded together and are water impermeable. They were made by surface thiol-Michael addition polymerisation, and gave a latent heat of 100-200Jg^{-1}. Schoth *et al*[38] fabricated polyurethane capsules containing sodium sulphate decahydrate using silica as emulsifier. The capsules produced were approximately 1µm in size with a ΔH of 58Jg^{-1}. Salaün *et al*[39,40] made microcapsules containing sodium phosphate dodecahydrate with a crosslinked polyurethane shell made up of cellulose acetate butyrate and methylene diisocyanate. Despite promising results,

Stephenson Institute for Renewable Energy, Department of Chemistry, University of Liverpool, Liverpool, UK, L69 7ZF. E-mail: m.graham2@liv.ac.uk

these capsules were prepared by complex methods, and have not displayed acceptable thermal cycling. To further improve their properties, PCM capsules should be nanosized (<1µm). This maximises surface-area-to-volume ratio, increasing heat transfer[41], reducing supercooling[42] and decreasing melting and freezing times[4]. Nanocapsules are also structurally stronger than microcapsules[4,43], and decreasing capsule size can lead to an increase in latent heat[44].

For this research, poly(ethyl-2-cyanoacrylate) (PECA) was chosen as shell material. Cyanoacrylates are highly reactive and have been used to encapsulate water soluble drugs since the 1980s. They spontaneously form nanocapsules 80-250nm in size[24,26,45–48] *via* anionic polymerisation upon addition to a water-in-oil (W/O) emulsion[49,50]. To fabricate nanocapsules, we used the *in situ* inverse miniemulsion polymerisation technique. We chose the salt hydrate magnesium nitrate hexahydrate ($Mg(NO_3)_2.6H_2O$) for this study, which has a melting temperature (T_M) of 89ºC, latent heat of 162.8Jg^{-1} and density of 1636kgm^{-3} in the solid state[16]. High density is a key property of salt hydrates, as a lower volume of the material is required to achieve high energy storage capacity. Paraffin waxes have a density of around 800kgm^{-3} by comparison. To the best of our knowledge, this work is the first time long-term cycling stability for encapsulated salt hydrates has been proven. Many investigations into salt hydrates suggested thickeners or nucleating agents must be added to prevent incongruent melting and supercooling[16,51]. Additives reduce the amount of salt hydrate per unit volume, leading to a decrease of latent heat. This study shows nanoencapsulation removes the need for any additives.

Experimental

Materials

$Mg(NO_3)_2.6H_2O$ (99% purity) was used as salt hydrate. Ethyl-2-cyanoacrylate (ECA) was employed as monomer. Tween 80 (polysorbate 80) and Span 20 (sorbitan monolaurate) were used as surfactants. Toluene and cyclohexane were used as oil for the continuous phase, and chloroform was used as solvent for the monomer. All materials were purchased from Sigma Aldrich UK and used without further purification. Milli-Q water was used throughout.

Methods

Preparation of PECA nanocapsules

PECA nanocapsules were prepared according to the method used by Kafka *et al*[24], which was in turn based on a well-established procedure[45,46,48]. An aqueous phase (1g) consisting of different $Mg(NO_3)_2.6H_2O$:water ratios (see Table 1), either solid or solubilised in water, was added to the continuous oil phase (9g) consisting of

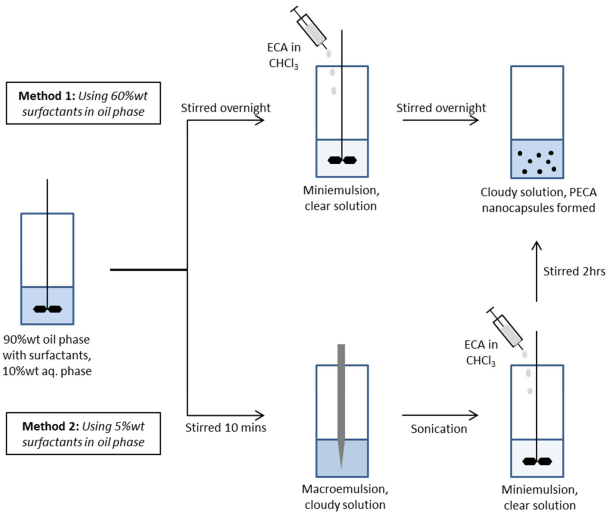

Fig. 1 – Synthesis of salt hydrate-loaded PECA nanocapsules by in situ polymerisation, employing mechanical stirring without (method 1) and with ultrasonic treatment (method 2).

60% weight percentage (wt) surfactants (3:2 blend of Tween 80:Span 20) and 40%wt toluene. The mixture was stirred overnight at 600 RPM to create a W/O miniemulsion. Then, ECA was dissolved in 3 times the amount of chloroform and added to the mixture dropwise. This was left to stir at 600 RPM overnight in an open vial. As chloroform evaporates, the polymerisation occurs around the microemulsion droplets. This procedure is outlined in Fig. 1 (Method 1). The capsules were separated by centrifugation (11000 RPM for 10 mins at 10ºC) and washed by redispersing in cyclohexane *via* sonication. The capsules were again centrifuged (6000 RPM for 5 mins at 10ºC), and the product left to dry at room temperature, giving a white powder.

Preparation of PECA nanocapsules with ultrasonic treatment

In order to decrease the amount of surfactants required, ultrasound was employed to create a W/O miniemulsion based on the method of Musyanovych *et al*[26]. Sonication can create miniemulsions due to the high energy from ultrasonic cavitation[28]. An aqueous phase (1g) containing $Mg(NO_3)_2.6H_2O$ in water (see Table 1) was added to an oil phase (9g) consisting of 5%wt surfactants and 95%wt cyclohexane. The mixture was mechanically stirred for 10 minutes at 600RPM to create a macroemulsion. This was then sonicated for 12 mins (30s on, 20s off pulse regime, 70% amplitude) with ice bath cooling, using a Qsonica Q700-220 sonicator (700W). During sonication the cloudy solution became almost transparent, signifying a stable W/O miniemulsion had formed. After sonication, ECA dissolved in 3 times the amount of chloroform was added dropwise and left to stir at 600 RPM in an open vial for around 2 hours. This procedure is outlined in Fig. 1 (Method 2). The product

Table 1 – Formulations of different capsule samples, NanoPCM3 was prepared using the ultrasonic method (Fig. 1, Method 2).

Sample	Oil Phase	Aqueous phase	ECA added
NanoPCM1	60%wt surfactants, 40%wt toluene	100%wt $Mg(NO_3)_2.6H_2O$	600µL
NanoPCM2	60%wt surfactants, 40%wt toluene	70%wt $Mg(NO_3)_2.6H_2O$, 30%wt H_2O	300µL
NanoPCM3	5%wt surfactants, 95%wt cyclohexane	20%wt $Mg(NO_3)_2.6H_2O$, 80%wt H_2O	200µL

was separated by centrifugation (11000RPM for 10 mins at 10°C) and left to dry at room temperature, yielding a translucent sticky solid. This was then redispersed in ethanol by sonication and centrifuged (6000 RPM for 5 mins at 10 °C). After drying at room temperature, a powder sample was obtained.

Characterisation

Capsule morphology and size measurements were taken using a JEOL JSM-7001F scanning electron microscope (SEM). Nanocapsule samples were prepared by dispersing in ethanol *via* bath sonication. 50µL of the dispersion was pipetted onto carbon tape on an aluminium SEM stub. Samples were dried at room temperature and coated with chromium before analysis. The $Mg(NO_3)_2.6H_2O$ sample was prepared by crushing the bulk material and adding to carbon tape on the SEM stub.

Chemical structure of the reagents and resulting nanocapsules was determined using Fourier transform infrared spectroscopy (FTIR), on a Bruker TENSOR II instrument equipped with an all reflective diamond ATR. Measurements were taken on transmittance mode with 64 scans from 400 to 4000cm^{-1}.

Differential scanning calorimetry (DSC) determined the latent heat storage properties and thermal cycling stability of the nanoPCMs. DSC was undertaken between 40 and 120°C for up to 100 cycles under a nitrogen atmosphere with a 5°C/min ramp, using a Perkin Elmer DSC6 .

Thermogravimetric analysis (TGA) experiments were done to obtain thermal degradation behaviour of the bulk $Mg(NO_3)_2.6H_2O$ and encapsulated NanoPCMs. TGA was undertaken using a TA Instruments SDT Q600 instrument. Measurements were taken from room temperature up to 800°C, with a ramp of 10°C/min under a nitrogen atmosphere.

Melting characteristics of the nanocapsules were compared to the bulk material. They were heated to 100°C *via* steam and allowed to cool back to room temperature. Photographs were taken before and after the heating to observe changes in macrostructure.

Results & Discussion

Chemical Structure of the NanoPCMs

SEM results are shown in Fig. 2. Pure $Mg(NO_3)_2.6H_2O$ is a crystalline solid with 10-50µm crystals (Fig. 2a). The nanocapsules (Fig. 2b-d) have a smooth surface, with complete coverage of the salt hydrate core by the polymer shell. No pores are present. The capsules are 100-200nm in size overall for all samples, which is consistent with previously reported sizes of PECA nanocapsules loaded with insulin[48]. Nanosized capsules not only improve thermal characteristics, but also improve diffusion tight bonding, which is an important factor in preventing leakage and maintaining hydration of the salt hydrate[4]. All nanocapsules are in the same size range, showing both methods were successful in obtaining stable inverse miniemulsions with similarly sized droplets.

Nanocapsules are structurally strong, indicated by the round shape of most capsules. This indicates the SEM high vacuum has little effect, whereas larger capsules may collapse due to the increased pressure[2]. A strong shell is important during practical application as the capsules must be pumped round the macroscale system.

FTIR spectra for $Mg(NO_3)_2.6H_2O$ & nanocapsule samples are shown in Fig. 3. Spectra for NanoPCM1 and NanoPCM2 are identical, so only the NanoPCM1 spectrum is shown. $Mg(NO_3)_2.6H_2O$ (Fig. 3a) has characteristic peaks for O-H stretching at 3356cm^{-1}, N=O bending at 1646 cm^{-1}, a mixture of N-O stretching and bending and N=O bend in the broad peak at 1365cm^{-1}, plus a sharp peak at 819 cm^{-1} for NO_3^-. NanoPCM1 (Fig. 3b) has peaks attributed to PECA - C-H stretch at 2927cm^{-1}, C=O at 1745cm^{-1} along with 2 C-O peaks at 1250 and 1013cm^{-1} signifying the presence of an ester group. Notably absent is a CN peak, which may be masked by the large amount of surfactants used to fabricate the samples.

NanoPCM3 (Fig. 3c) has a similar spectrum to NanoPCM1 & 2 with respect to PECA, with peaks at 2923, 1745, 1253 and 1079cm^{-1}, respectively. It also has a peak for CN at 2360cm^{-1}. Peaks attributed to $Mg(NO_3)_2.6H_2O$ are more pronounced in the spectrum for NanoPCM3 at 3373, 1643, 1345 and 827cm^{-1}. This suggests there is

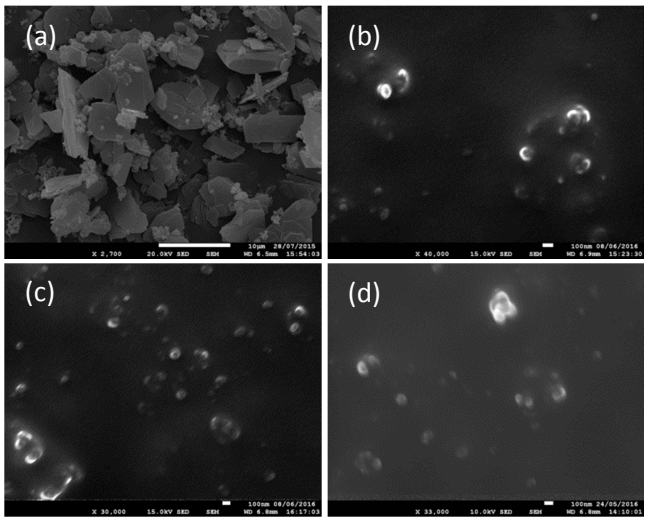

Fig. 2 - SEM micrographs of (a) bulk $Mg(NO_3)_2.6H_2O$, (b)NanoPCM1, (c) NanoPCM2 and (d) NanoPCM3. Scale bar for (a) is 10µm, for (b-d) 100nm.

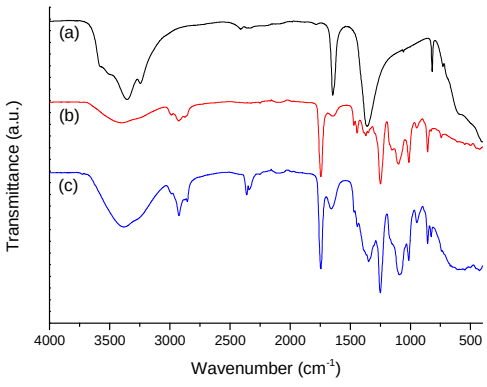

Fig. 3 - FTIR spectra for (a) $Mg(NO_3)_2.6H_2O$ (b) NanoPCM1 and (c) NanoPCM3.

more $Mg(NO_3)_2.6H_2O$ present in this sample due to increased encapsulation efficiency. It also indicates the encapsulated salt hydrate has a similar composition to the bulk material. There are some minor wavenumber shifts for the $Mg(NO_3)_2.6H_2O$ when encapsulated. These shifts are caused by spatial confinement, which affects H-bonding in the salt hydrate core.

Thermal Analysis

TGA curves are shown in Fig. 4. $Mg(NO_3)_2.6H_2O$ starts to lose mass at around 70°C and has lost 36% mass by 160°C, which corresponds to water loss. Remaining mass was lost from 300 to 460°C. According to literature, $Mg(NO_3)_2.6H_2O$ decomposes at 330°C. 14% mass remains after 800°C, mainly consisting of magnesium oxide. Magnesium makes up 10% mass of $Mg(NO_3)_2.6H_2O$.

NanoPCM1 and NanoPCM2 have very similar curves due to their nearly identical synthesis. Both lose 4% mass by 150°C, attributed to water evaporating. From 150-300°C the PECA shell decomposes, which is in agreement with previous research[52]. NanoPCM1 and NanoPCM2 lose 60% and 55% mass, respectively, over this temperature range. The higher % mass loss from NanoPCM1 indicates the sample contained more shell material, which is expected due to the higher amount of monomer added during synthesis. Both samples then lose mass from 330-400°C due to the magnesium nitrate decomposing. After heating to 800°C, NanoPCM1 has 2% mass remaining, while NanoPCM2 has 8%. Remaining mass consists of magnesium oxide present in the sample along with carbon residue. The higher remaining mass after 800°C proves a larger amount of salt hydrate was present in the NanoPCM2 sample.

NanoPCM3 loses mass more rapidly from 30-150°C (12% mass loss) compared to NanoPCM1 & 2, due to extra water in the aqueous phase evaporating. There is an increase in the rate of mass loss at 150°C, corresponding with the decomposition of the PECA shell. The shell degrades more slowly than the other NanoPCMs, as shown by the less steep curve. This shows a higher molecular weight (MW) shell was formed due to reduced surfactant quantity used in the synthesis[26]. High MW shells are desirable due to improved strength and potential for higher encapsulation efficiency[53]. A further increase in the rate of mass loss occurs starting at 330°C as the salt degrades. After heating to 800°C, there is 14% mass remaining, more than NanoPCM1 & 2. Therefore, there is more $Mg(NO_3)_2.6H_2O$ encapsulated in NanoPCM3.

DSC results in Fig. 5 show that the PECA shell vastly increases thermal cycling stability of the salt hydrate. The thermogram for bulk $Mg(NO_3)_2.6H_2O$ (Fig. 5a) has a latent heat of 160.2Jg^{-1} and a melting point with $T_{onset,\ M}$ = 88°C and T_M = 93°C, slightly differing from literature values of 162.8Jg^{-1} and 89 °C[16]. There are 2 freezing peaks, one at $T_{onset,\ F}$ = 77°C and T_F = 74°C and a smaller freezing peak at $T_{onset,\ F}$ = 68°C and T_F = 66°C. The smaller peak can be attributed to a solid-solid transition. After 5 cycles, the melting and freezing peaks are severely decreased, and after 10 cycles signals are lost completely as the PCM completely dehydrates to $Mg(NO_3)_2$ salt. This instability, coupled with supercooling ($T_{onset,\ M} - T_{onset,\ F}$) of

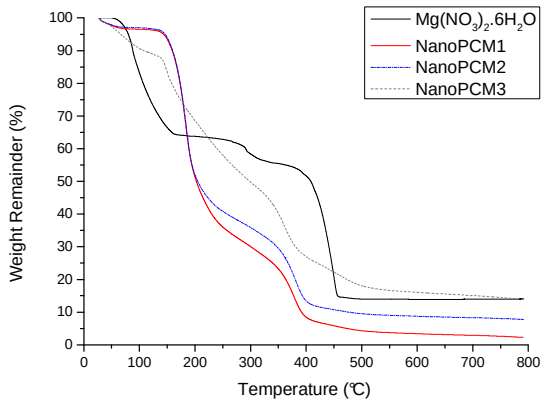

Fig. 4 - TGA curves for $Mg(NO_3)_2.6H_2O$ & NanoPCMs.

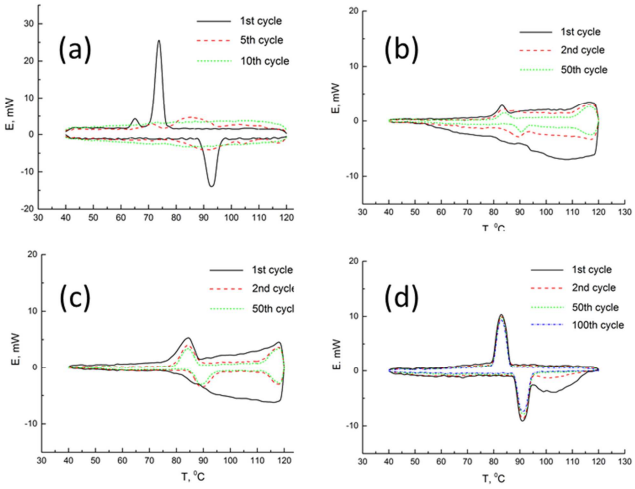

Fig. 5 - DSC thermograms for (a) bulk $Mg(NO_3)_2.6H_2O$ (b) NanoPCM1 (c) NanoPCM2 and (d) NanoPCM3.

around 11°C, demonstrates the inherent problems of salt hydrates.

In the 1st cycle for NanoPCM1 and NanoPCM2 (Fig. 5b & c), there is a broad endothermic peak between approximately 60°C-120°C and 80°C-120°C, respectively. This can be attributed to evaporation of excess water present which is not associated to the salt hydrate. Excess water is located within damaged nanocapsules or outside the capsule structure. NanoPCM1 still has excess water evaporating during the 2nd cycle, whereas for NanoPCM2 this only occurs on the first cycle. This suggests more water is associated to the salt hydrate in NanoPCM2, so cannot freely evaporate. As extra water (30%wt) was added to the aqueous phase of NanoPCM2, it can be concluded the extra water helps preserve salt hydrate composition after encapsulation. Previous research has shown extra water helps prevent dehydration of the salt[6,54]. For both samples, there are two peaks present for both melting and freezing. The peaks are attributed to $Mg(NO_3)_2.6H_2O$ and $Mg(NO_3)_2.2H_2O$ (T_M - 129°C), the two stable hydrated forms of magnesium nitrate. $Mg(NO_3)_2.2H_2O$ is formed by incongruent melting of $Mg(NO_3)_2.6H_2O$, shown in Eqs. 1 and 2. The formation of a lower hydrate from incongruent melting is irreversible[13,55]. The presence of both the hexahydrate and dihydrate is not desirable, as this leads to 2 different T_Ms with low

$$Mg(NO_3)_2.6H_2O \underset{<90^oC}{\overset{90^oC}{\rightleftharpoons}} Mg(NO_3)_2 + 6H_2O$$

Eq. 1 Congruent melting of $Mg(NO_3)_2.6H_2O$

$$1.\ Mg(NO_3)_2.6H_2O \xrightarrow{90^oC} Mg(NO_3)_2.2H_2O + 4H_2O$$

$$2.\ Mg(NO_3)_2.2H_2O \underset{<129^oC}{\overset{129^oC}{\rightleftharpoons}} Mg(NO_3)_2 + 2H_2O$$

Eq. 2 Incongruent melting of $Mg(NO_3)_2.6H_2O$, occurring in 2 stages.

latent heat (after 50 cycles, 26.3Jg^{-1} for NanoPCM1 and 39.4Jg^{-1} for NanoPCM2).

NanoPCM3 displays the best results (Fig. 5d) with a latent heat of 83.2Jg^{-1} after 50 cycles, $T_{onset,\ M}$ = 87°C, T_M = 91°C and $T_{onset,\ F}$ = 86°C, T_F = 83°C. Supercooling is only 1°C. The broad peak for the evaporation of excess water is shifted to around 95°C. This water loss may be from capsules damaged during formation of the capsule shell. The presence of only one T_M at 91°C shows only $Mg(NO_3)_2.6H_2O$ forms within the NanoPCM3 core. The T_M remains constant at 91°C during repeated thermal cycling, whereas with encapsulated paraffin waxes the T_M can fluctuate[56]. Incongruent melting was therefore prevented by the constrained capsule environment. A constant T_M is important, as PCMs work over a small temperature range during practical application. NanoPCM3 demonstrates constant latent heat at 50 and 100 cycles, with only a 3% decrease after the 1st cycle, showing encapsulation promotes long term stability and sufficient elasticity during phase transition of the salt hydrate core. According to the ratio between latent heat of the encapsulated salt hydrate and bulk salt hydrate, the encapsulation efficiency is 52%. The improved thermal properties of NanoPCM3 prove that use of sonication to form the initial inverse miniemulsion is of great benefit. Supercooling is vastly reduced by encapsulation, illustrating how the nanoscale size of the PCM-loaded core improves heat transfer compared to bulk $Mg(NO_3)_2.6H_2O$.

Chemical Stability of the NanoPCMs

To determine chemical stability of NanoPCM3 during long-term use, an FTIR spectrum was taken after 100 melting/freezing cycles between 50-120°C (Fig. 6). The spectrum is almost identical after thermal cycling, with no new peaks formed. Both the main peaks for $Mg(NO_3)_2.6H_2O$ (O-H stretching at 3373cm^{-1}, N=O bending at 1643cm^{-1}, a mix of N-O stretching and bending and N=O bend in the broad peak at 1345cm^{-1} and NO_3^- at 827cm^{-1}) and peaks related to PECA (C-H stretch at 2923cm^{-1}, C=O at 1745cm^{-1} and 2 C-O peaks at 1253 and 1079cm^{-1}) are present in the NanoPCM3 spectrum after 100 thermal cycles, indicating chemical stability of PCM nanocapsules during storage and release of latent heat.

To check the macroscale appearance of the bulk $Mg(NO_3)_2.6H_2O$ in

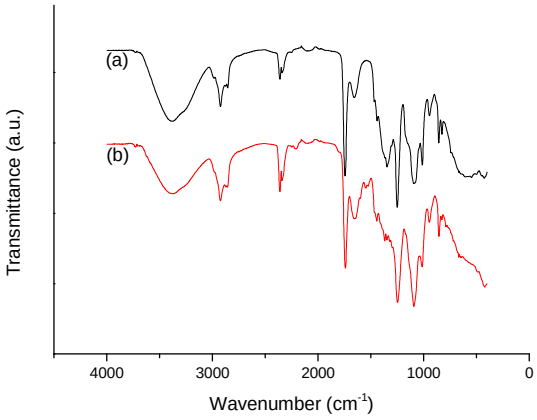

Fig. 6 - FTIR spectra for NanoPCM3 (a) before and (b) after 100 thermal cycles.

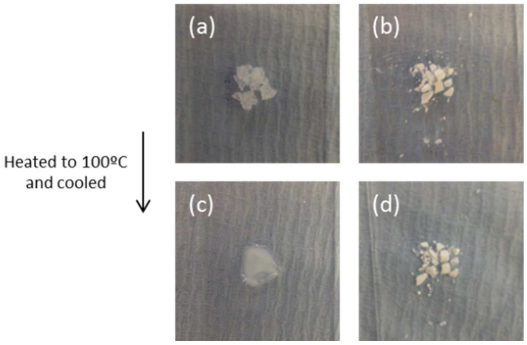

Fig. 7 - Pictures of $Mg(NO_3)_2.6H_2O$ (a & c) and nanoencapsulated salt hydrate (b & d) before heating to 100°C (top), and after letting them cool back to room temperature (bottom).

comparison with its encapsulated form, both samples were heated to 100°C and were then cooled back to room temperature. The results are shown in Fig. 7.

Before melting, $Mg(NO_3)_2.6H_2O$ is a crystalline solid (Fig. 7a). After melting, it recrystallizes to the solid shown in Fig. 7c. This solid is surrounded by water, showing a volume change occurs during phase transition. The recrystallized solid forms a compact block, which prevents free diffusion of water vapour[57]. This mechanism leads to changes in hydration of $Mg(NO_3)_2.6H_2O$, eventually resulting in the formation of $Mg(NO_3)_2$ salt.

In contrast to the bulk material, nanoencapsulated salt hydrates (Fig. 7b & d) show no volume increase or change in appearance before and after heating to 100°C. This indicates chemical and structural stability at the transition temperature. The absence of leakage means the salt hydrate is fully protected by encapsulation from the outside environment, which helps prevent changes in salt hydrate composition of nanocapsule powder on the macroscale. These observations are consistent with the thermal stability shown by DSC.

Conclusions

$Mg(NO_3)_2.6H_2O$ phase change material was successfully encapsulated into poly(ethyl-2-cyanoacrylate) nanocapsules of 100-

200nm in size by *in situ* inverse miniemulsion polymerisation. FTIR analysis confirmed the presence of $Mg(NO_3)_2.6H_2O$ in the core of the nanocapsules. Inverse miniemulsions produced by mechanical stirring required large amounts of surfactant to stabilise, and led to nanocapsules with two T_Ms due to partial incongruent melting. Employing ultrasound to create the inverse miniemulsion improved the synthesis, greatly reducing the required amount of surfactant and led to capsules containing with one T_M of 91ºC, showing only $Mg(NO_3)_2.6H_2O$ was present. DSC results demonstrated for the first time high thermal stability of the nanoencapsulated salt hydrates, which remained unchanged after 100 thermal cycles with a latent heat of $83.2Jg^{-1}$. Chemical and macroscale stability of the nanoencapsulated salt hydrates were also proven by FTIR and visual observations after heating/cooling cycles. The thermal properties of the nanocapsules are a great improvement over the bulk $Mg(NO_3)_2.6H_2O$, which loses its structural integrity and chemical composition after only 5 cycles.

Salt hydrate PCMs with long lifetimes are important for future energy storage applications, due to their high heat capacity and cost effectiveness compared to commonly used paraffin wax PCMs. Efficient energy storage has the potential to greatly reduce global energy demand, providing a sustainable future. Therefore, more studies are required in future to maximise encapsulation yield and thermal properties of the nanocapsules loaded with cheap salt hydrate PCMs with high latent heat density. Future work will also focus on how encapsulation of the salt hydrate reduces their corrosiveness towards container materials.

Acknowledgements

We thank Prof. Katharina Landfester (Max Planck Institute for Polymer Research) for stimulating discussions on PCM encapsulation at the planning stage of the work. This research was supported by the ERC Enercapsule project.

References

1 C. Rathgeber, H. Schmit, P. Hennemann and S. Hiebler, *Appl. Energy*, 2014, **136**, 7–13.
2 P. Felix De Castro and D. G. Shchukin, *Chem. - A Eur. J.*, 2015, **21**, 11174–11179.
3 D. C. Hyun, N. S. Levinson, U. Jeong and Y. A. Xia, *Angew. Chemie-International Ed.*, 2014, **53**, 3780–3795.
4 P. B. Salunkhe and P. S. Shembekar, *Renew. Sustain. Energy Rev.*, 2012, **16**, 5603–5616.
5 M. Kenisarin and K. Mahkamov, *Renew. Sustain. Energy Rev.*, 2007, **11**, 1913–1965.
6 A. A. El-Sebaii, S. Al-Heniti, F. Al-Agel, A. A. Al-Ghamdi and F. Al-Marzouki, *Energy Convers. Manag.*, 2011, **52**, 1771–1777.
7 B. Zalba, J. M. Marin, L. F. Cabeza and H. Mehling, *Appl. Therm. Eng.*, 2003, **23**, 251–283.
8 V. V. Tyagi and D. Buddhi, *Renew. Sustain. Energy Rev.*, 2007, **11**, 1146–1166.
9 M. J. Huang, P. C. Eames and B. Norton, *Int. J. Heat Mass Transf.*, 2004, **47**, 2715–2733.
10 A. Hasan, S. J. McCormack, M. J. Huang, J. Sarwar and B. Norton, *Sol. Energy*, 2015, **115**, 264–276.
11 F. L. Tan and C. P. Tso, *Appl. Therm. Eng.*, 2004, **24**, 159–169.
12 E. M. Alawadhi and C. H. Amon, *IEEE Trans. Components Packag. Technol.*, 2003, **26**, 116–125.
13 A. Abhat, *Sol. Energy*, 1983, **30**, 313–332.
14 B. Xu, P. Li and C. Chan, *Appl. Energy*, 2015, **160**, 286–307.
15 C. Liu, F. Li, L. P. Ma and H. M. Cheng, *Adv. Mater.*, 2010, **22**, E28–E62.
16 M. M. Farid, A. M. Khudhair, S. A. K. Razack and S. Al-Hallaj, *Energy Convers. Manag.*, 2004, **45**, 1597–1615.
17 D. W. Hawes, D. Feldman and D. Banu, *Energy Build.*, 1993, **20**, 77–86.
18 T. Khadiran, M. Z. Hussein, Z. Zainal and R. Rusli, *Sol. Energy Mater. Sol. Cells*, 2015, **143**, 78–98.
19 L. F. Cabeza, J. Illa, J. Roca, F. Badia, H. Mehling, S. Hiebler and F. Ziegler, *Mater. Corros.*, 2001, **52**, 140–146.
20 D. Z. Yin, L. Ma, J. J. Liu and Q. Y. Zhang, *Energy*, 2014, **64**, 575–581.
21 D. G. Shchukin and H. Möhwald, *Adv. Funct. Mater.*, 2007, **17**, 1451–1458.
22 D. G. Shchukin, M. Zheludkevich, K. Yasakau, S. Lamaka, M. G. S. Ferreira and H. Möhwald, *Adv. Mater.*, 2006, **18**, 1672–1678.
23 D. Chitkara and N. Kumar, *Pharm. Res.*, 2013, **30**, 2396–2409.
24 A. P. Kafka, B. J. McLeod, T. Rades and A. McDowell, *J. Control. Release*, 2011, **149**, 307–313.
25 S. Vrignaud, N. Anton, C. Passirani, J. P. Benoit and P. Saulnier, *Drug Dev Ind Pharm*, 2013, **39**, 1706–1711.
26 A. Musyanovych and K. Landfester, *Prog. Colloid Polym. Sci.*, 2007, **134**, 120–127.
27 A. P. R. Johnston, C. Cortez, A. S. Angelatos and F. Caruso, *Curr. Opin. Colloid Interface Sci.*, 2006, **11**, 203–209.
28 N. Anton, J. P. Benoit and P. Saulnier, *J. Control. Release*, 2008, **128**, 185–199.
29 M. Antonietti and K. Landfester, *Prog. Polym. Sci.*, 2002, **27**, 689–757.
30 S. Freitas, H. P. Merkle and B. Gander, *J. Control. Release*, 2005, **102**, 313–332.
31 J. M. Asua, *Prog. Polym. Sci.*, 2014, **39**, 1797–1826.
32 A. Sari, C. Alkan, A. Karaipekli and O. Uzun, *Sol. Energy*, 2009, **83**, 1757–1763.
33 K. Tumirah, M. Z. Hussein, Z. Zulkarnain and R. Rafeadah, *Energy*, 2014, **66**, 881–890.
34 M. G. de Cortazar and R. Rodriguez, *J. Appl. Polym. Sci.*, 2013, **127**, 5059–5064.
35 Z. Zheng, J. Jin, G.-K. Xu, J. Zou, U. Wais, A. Beckett, T. Heil, S. Higgins, L. Guan, Y. Wang and D. Shchukin, *ACS Nano*, 2016, **10**, 4695–4703.
36 J. Huang, T. Y. Wang, P. P. Zhu and J. B. Xiao, *Thermochim. Acta*, 2013, **557**, 1–6.
37 D. Platte, U. Helbig, R. Houbertz and G. Sextl, *Macromol. Mater. Eng.*, 2013, **298**, 67–77.
38 A. Schoth, K. Landfester and R. Muñoz-Espí, *Langmuir*, 2015, **31**, 3784–3788.
39 F. Salaün, E. Devaux, S. Bourbigot and P. Rumeau, *Carbohydr. Polym.*, 2008, **73**, 231–240.
40 F. Salaün, E. Devaux, S. Bourbigot and P. Rumeau, *Carbohydr. Polym.*, 2010, **79**, 964–974.
41 Z. H. Chen, F. Yu, X. R. Zeng and Z. G. Zhang, *Appl. Energy*, 2012, **91**, 7–12.
42 Y. Wang, Y. Zhang, T. Xia, W. Zhao and W. Yang, *Sol. Energy Mater. Sol. Cells*, 2014, **120**, 481–490.
43 A. Jamekhorshid, S. M. Sadrameli and M. Farid, *Renew. Sustain. Energy Rev.*, 2014, **31**, 531–542.
44 P. F. De Castro, A. Ahmed and D. G. Shchukin, *Chem. - A Eur. J.*,

2016, **22**, 4389–4394.
45 M. R. Gasco and M. Trotta, *Int. J. Pharm.*, 1986, **29**, 267–268.
46 N. Behan, C. Birkinshaw and N. Clarke, *Biomaterials*, 2001, **22**, 1335–1344.
47 T. Pitaksuteepong, N. M. Davies, I. G. Tucker and T. Rades, *Eur. J. Pharm. Biopharm.*, 2002, **53**, 335–342.
48 S. Watnasirichaikul, N. M. Davies, T. Rades and I. G. Tucker, *Pharm. Res.*, 2000, **17**, 684–689.
49 F. Chouinard, F. W. K. Kan, J. C. Leroux, C. Foucher and V. Lenaerts, *Int. J. Pharm.*, 1991, **72**, 211–217.
50 S. Vrignaud, J. P. Benoit and P. Saulnier, *Biomaterials*, 2011, **32**, 8593–8604.
51 M. Telkes, *Ind. Eng. Chem.*, 1952, **44**, 1308–1310.
52 M. G. Han, S. Kim and S. X. Liu, *Polym. Degrad. Stab.*, 2008, **93**, 1243–1251.
53 U. Paiphansiri, P. Tangboriboonrat and K. Landfester, *Macromol. Biosci.*, 2006, **6**, 33–40.
54 D. R. Biswas, *Sol. Energy*, 1977, **19**, 99–100.
55 L. F. Cabeza, a. Castell, C. Barreneche, a. De Gracia and a. I. Fernández, *Renew. Sustain. Energy Rev.*, 2011, **15**, 1675–1695.
56 C. Alkan, A. Sari, A. Karaipekli and O. Uzun, *Sol. Energy Mater. Sol. Cells*, 2009, **93**, 143–147.
57 A. Solé, I. Martorell and L. F. Cabeza, *Renew. Sustain. Energy Rev.*, 2015, **47**, 386–398.